

Discovery of three new transiting hot Jupiters: WASP-161 b, WASP-163 b and WASP-170 b

K. BARKAOUI,^{1,2} A. BURDANOV,¹ C. HELLIER,³ M. GILLON,¹ B. SMALLEY,³ P. F. L. MAXTED,³ M. LENDL,^{4,5}
A. H. M. J. TRIAUD,⁶ D. R. ANDERSON,³ J. MCCORMAC,⁷ E. JEHIN,¹ Y. ALMLEAKY,^{8,9} D. J. ARMSTRONG,⁷
Z. BENKHALDOUN,² F. BOUCHY,⁵ D. J. A. BROWN,⁷ A. C. CAMERON,¹⁰ A. DAASSOU,² L. DELREZ,^{11,1} E. DUCROT,¹
E. FOXELL,⁷ C. MURRAY,¹¹ L. D. NIELSEN,⁵ F. PEPE,⁵ D. POLLACCO,⁷ F. J. POZUELOS,¹ D. QUELOZ,^{11,5} D. SEGRANSAN,⁵
S. UDRY,⁵ S. THOMPSON,¹¹ AND R. G. WEST⁷

¹*Space sciences, Technologies and Astrophysics Research (STAR) Institute, Université de Liège, Belgium*

²*Oukaimeden Observatory, High Energy Physics and Astrophysics Laboratory, Cadi Ayyad University, Marrakech, Morocco*

³*Astrophysics Group, Keele University, Staffordshire, ST5 5BG, UK*

⁴*Space Research Institute, Austrian Academy of Sciences, Schmiedlstr. 6, 8042 Graz, Austria*

⁵*Observatoire astronomique de l'Université de Geneve, 51 ch. des Maillettes, 1290 Sauverny, Switzerland*

⁶*School of Physics & Astronomy, University of Birmingham, Edgbaston, Birmingham B15 2TT, United Kingdom*

⁷*Department of Physics, University of Warwick, Gibbet Hill Road, Coventry, CV4 7AL, UK*

⁸*Space and Astronomy Department, Faculty of Science, King Abdulaziz University, 21589 Jeddah, Saudi Arabia*

⁹*King Abdullah Centre for Crescent Observations and Astronomy, Makkah Clock, Mecca 24231, Saudi Arabia*

¹⁰*School of Physics and Astronomy, University of St Andrews, North Haugh, St Andrews, Fife KY16 9SS*

¹¹*Cavendish Laboratory, J J Thomson Avenue, Cambridge, CB3 0HE, UK*

ABSTRACT

We present the discovery by the WASP-South transit survey of three new transiting hot Jupiters, WASP-161 b, WASP-163 b and WASP-170 b. Follow-up radial velocities obtained with the Euler/CORALIE spectrograph and high-precision transit light curves obtained with the TRAPPIST-North, TRAPPIST-South, SPECULOOS-South, NITES, and Euler telescopes have enabled us to determine the masses and radii for these transiting exoplanets. WASP-161 b completes an orbit around its $V = 11.1$ F6V-type host star in 5.406 days, and has a mass and radius of $2.5 \pm 0.2 M_{Jup}$ and $1.14 \pm 0.06 R_{Jup}$ respectively. WASP-163 b has an orbital period of 1.609 days, a mass of $1.9 \pm 0.2 M_{Jup}$, and a radius of $1.2 \pm 0.1 R_{Jup}$. Its host star is a $V = 12.5$ G8-type dwarf. WASP-170 b is on a 2.344 days orbit around a G1V-type star of magnitude $V = 12.8$. It has a mass of $1.7 \pm 0.2 M_{Jup}$ and a radius of $1.14 \pm 0.09 R_{Jup}$. Given their irradiations ($\sim 10^9 \text{ erg.s}^{-1}.\text{cm}^{-2}$) and masses, the three new planets' sizes are in good agreement with classical structure models of irradiated giant planets.

Keywords: planetary systems- stars: WASP-161, WASP-163 and WASP-170- techniques: photometric- techniques: radial velocities-techniques: spectroscopic

1. INTRODUCTION

naugurated by the seminal discovery of 51 Peg b in 1995 (Mayor and Queloz 1995), the study of exoplanets has dramatically developed to become one of the most important fields of modern astronomy. Since 1995, several thousand exoplanets have been detected at an ever-increasing pace (NASA Exoplanet Archive), most of them by the transit technique that relies on the partial occultation of the host star by its planet (Charbonneau et al. 2000; Henry et al. 2000). Among this large harvest, highly irradiated giant planets (aka hot Jupiters) transiting bright nearby stars have a particular scientific interest. These rare objects - $\sim 1\%$ of solar-type stars (Winn and Fabrycky 2015) - undergo irradiation orders of magnitude larger than any solar system planets (Fortney et al. 2007), and are also subject to intense gravitational and magnetic fields (Correia and Laskar 2010; Chang et al. 2010). Studying in detail their physical and chemical response to such extreme conditions provides a unique opportunity to improve our knowledge on planetary structure, composition and physics. The brightness of their host star combined to their eclipsing configuration

makes possible such detailed characterization, notably to measure precisely their size, mass, and orbital parameters (Winn 2010; Deming and Seager 2009), but also to probe their atmospheric properties (chemical composition, vertical pressure-temperature profiles, albedos, and circulation patterns) (Seager and Deming 2010; Sing et al. 2016; Crossfield 2015).

The WASP (Wide Angle Search for Planets) project (Pollacco et al. 2006; Collier Cameron et al. 2007) uses two robotic installations, one at La Palma (Canary Islands, Spain) and one at Sutherland (South Africa), to scout the sky for gas giants transiting stars in the V -magnitude range $9 \sim 13$. With more than 100 hot Jupiters discovered so far in front of bright nearby stars, WASP is a key contributor to the study of highly irradiated giant planets. In this paper, we report the discovery by the Southern WASP station of three new gas giants, WASP-161 b, WASP-163 b and WASP-170 b, transiting bright ($V = 11.1, 12.5$ & 12.8) solar-type (F6-, G8- and G1-type) dwarf stars.

In Section 2, we present the observations used to discover WASP-161 b, WASP-163 b and WASP-170 b, and to confirm their planetary natures and measure their parameters. In Section 2.2.1, we describe notably TRAPPIST-North, a 60cm robotic telescope installed recently by the University of Liège at Oukaimeden observatory (Morocco), that played a significant role in the confirmation and characterization of the planets. Section 3.1 presents the determination of the atmospheric parameters of the host stars. In Section 3.2, we describe our global analysis of the dataset for the three planetary systems that enabled us to determine their main physical and orbital parameters. We discuss briefly our results in Section 6.

2. OBSERVATIONS AND DATA REDUCTION

2.1. WASP photometry

WASP-161 and WASP-170 (see Table 1 for coordinates and magnitudes) were observed by WASP-South (Hellier et al. 2011, 2012) in 2011 and 2012, while WASP-163 was observed in 2010 and 2012. The pipeline-processed photometric measurements were detrended and searched for transits using the methods described by Collier Cameron et al. (2006), and selected (Collier Cameron et al. 2007) as valuable candidates showing possible transits of short-period ($\sim 5.4, 1.6$, and 2.3 days) planetary sizes bodies (Fig. 1).

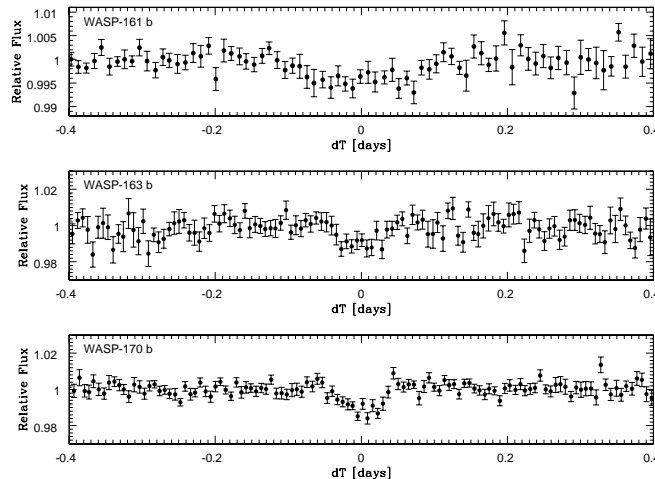


Figure 1. WASP photometry for WASP-161 (top), WASP-163 (middle) and WASP-170 (bottom) folded on the best-fitting transit ephemeris from the transit search algorithm presented in Collier Cameron et al. (2006), and binned per 10 min intervals.

2.2. Follow-up Photometry

2.2.1. TRAPPIST-North

TRAPPIST-North is a 60 cm robotic telescope installed in spring 2016 at Oukaimeden Observatory in Morocco. It is an instrumental project led by the University of Liège (Belgium) and conducted in collaboration with the Cadi Ayyad University of Marrakech (Morocco). TRAPPIST-North extends the TRAPPIST project to the Northern

Star general informations			
	WASP-161	WASP-163	WASP-170
	2MASS08252108-1130035	2MASS17060901-1024467	2MASS09013992-2043133
	GaiaId 5751177091580191360	GaiaId 4334991786994866304	GaiaId 5656184406542140032
RA (J200)	08 ^h 25 ^m 21.09 ^s	17 ^h 06 ^m 08.98 ^s	09 ^h 01 ^m 39.93 ^s
Dec (J200)	-11°30′03.6″	-10°24′47.0″	-20°43′13.6″
Vmag	11.09	12.54	12.79
Jmag	10.09	10.67	11.13
Stellar parameters from spectroscopic analysis			
T_{eff} (K)	6400 ± 100	5500 ± 200	5600 ± 150
log g_*	4.5 ± 0.15	4.0 ± 0.3	4.0 ± 0.2
[Fe/H]	+0.16 ± 0.09	-0.34 ± 0.21	+0.22 ± 0.09
Spectral type	F6	G8	G1
$V \sin i$ [Km/s]	18 ± 0.8	< 5	5.6 ± 1
log $A(Li)$	No Lithium seen	< 1.6	1.52 ± 0.09
Parameters from MCMC analysis			
Jump parameters			
Planet/star area ratio $(R_p/R_*)^2$ [%]	0.45092 ± 0.00023	1.417 ± 0.067	1.382 ± 0.001
$b' = a \cos i_p / R_*$ [R_*]	0.14 ^{+0.15} _{-0.10}	0.45 ^{+0.09} _{-0.06}	0.689 ± 0.021
Transit duration W [d]	0.2137 ± 0.0022	0.093 ± 0.001	0.085 ± 0.001
T_0 [HJD]	7416.5289 ± 0.0011	7918.4620 ± 0.0004	7802.3915 ± 0.0002
Orbital period P [d]	5.4060425 ± 0.0000048	1.6096884 ± 0.0000015	2.34478022 ± 0.0000036
RV K_2 [m.s ⁻¹ d ^{1/3}]	405 ± 20	386.69 ± 16	340 ± 20
Effective temperature T_{eff} [K]	6406 ± 100	5499 ± 200	5593 ± 150
Metallicity [Fe/H]	0.16 ± 0.09	-0.34 ± 0.21	0.21 ± 0.19
Deduced stellar parameters			
Mean density ρ_*	0.282 ^{+0.013} _{-0.027}	0.92 ^{+0.13} _{-0.10}	1.121 ^{+0.093} _{-0.076}
Stellar surface gravity log g_*	4.111 ^{+0.023} _{-0.033}	4.411 ^{+0.042} _{-0.040}	4.466 ± 0.031
Stellar mass M_* [M_\odot]	1.39 ± 0.14	0.97 ± 0.15	0.93 ± 0.15
Stellar radius R_* [R_\odot]	1.712 ^{+0.083} _{-0.072}	1.015 ^{+0.071} _{-0.074}	0.938 ^{+0.056} _{-0.061}
Luminosity L_* [L_\odot]	4.44 ^{+0.56} _{-0.48}	0.84 ^{+0.20} _{-0.17}	0.77 ± 0.14
Deduced planet parameters			
	WASP-161 b	WASP-163 b	WASP-170 b
RV K [ms ⁻¹]	230 ± 12	329 ± 14	255 ± 15
Planet/star radius ratio R_p/R_*	0.0671 ± 0.0017	0.119 ± 0.003	0.1175 ± 0.0041
Impact parameter b [R_*]	0.14 ^{+0.15} _{-0.10}	0.448 ^{+0.063} _{-0.094}	0.689 ± 0.021
Scaled semi-major axis a/R_*	8.49 ^{+0.13} _{-0.28}	5.62 ^{+0.26} _{-0.21}	7.71 ^{+0.21} _{-0.18}
Orbital semi-major axis a [AU]	0.0673 ± 0.0023	0.0266 ± 0.0014	0.0337 ± 0.0018
Orbital inclination i_p [deg]	89.01 ^{+0.69} _{-1.0}	85.42 ^{+1.10} _{-0.85}	84.87 ± 0.28
Density ρ_p [ρ_{Jup}]	1.66 ± 0.22	1.07 ^{+0.23} _{-0.17}	1.21 ^{+0.24} _{-0.19}
Surface gravity log g_p [cgs]	3.69 ^{+0.37} _{-0.42}	3.52 ± 0.05	3.54 ± 0.05
Mass M_p [M_{Jup}]	2.49 ± 0.21	1.87 ± 0.21	1.6 ± 0.2
Radius R_p [R_{Jup}]	1.143 ^{+0.065} _{-0.058}	1.202 ± 0.097	1.096 ± 0.085
Roche limit a_R [AU]	0.01101 ^{+0.00075} _{-0.00068}	0.011 ± 0.001	0.011 ± 0.001
a/a_R	6.12 ^{+0.25} _{-0.28}	2.35 ^{+0.16} _{-0.13}	3.15 ± 0.19
Equilibrium temperature T_{eq} [K]	1557 ⁺³⁴ ₋₂₉	1638 ± 68	1422 ± 42
Irradiation [erg.s ⁻¹ .cm ⁻²]	1.35 ^{+0.34} _{-0.26} × 10 ⁹	1.63 ± 0.45 × 10 ⁹	9.3 ^{+2.3} _{-2.5} × 10 ⁸

Table 1. The parameters of the WASP-161, WASP-163, and WASP-170 planetary systems (values + 1 σ error bars).

hemisphere, and, as its Southern twin TRAPPIST-South, is fully dedicated to the study of planetary systems via two complementary approaches: the detection and characterization of transiting exoplanets, and the study of comets and other small bodies in the Solar System. The exoplanet program of TRAPPIST (75% of its observational time) is dedicated to several programs: participating to the SPECULOOS project that aims to explore the nearest ultracool dwarf stars for transiting terrestrial planets (Gillon et al. 2017; Gillon 2018; Burdanov et al. 2017; Delrez et al. 2018); the search for the transit of planets previously detected by radial velocity (Bonfils et al. 2011); the follow-up of transiting planets of high interest (e.g. Gillon et al. 2012); and the follow-up of transiting planet candidates identified by wide-field transit surveys like WASP (e.g. Delrez et al. 2014). TRAPPIST-North has a F/8 Ritchey-Chretien optical design. It is fully automated and is protected by a 4.2 meters diameter dome equipped with a weather station and independent rain and light sensors. It is equipped with a thermoelectrically-cooled 2048×2048 deep-depletion Andor IKONL BEX2 DD CCD camera that has a pixel scale of $0.60''$ that translates into a field of view of $19.8' \times 19.8'$. It is coupled to a direct-drive mount of German equatorial design. We refer the reader to Jehin et al. (2011) for more technical details and performances of the TRAPPIST telescopes.

TRAPPIST-North observed two partial transits of WASP-161 b in the Sloan- z' filter (20 Dec 2017 and 12 Feb 2018), two partial transits and one full transit of WASP-163 b in the $I + z$ filter (24 Apr, 02 May, and 13 Jun 2017), and three partial transits of WASP-170 b in the $I + z$ (19 Apr 2017 and 11 Jan 2018) and V (17 Feb 2017) filters. The reduction and photometric analysis of the data were performed as described in Gillon et al. (2013). The resulting light curves are shown in Fig. 2, 3, and 4.

2.2.2. TRAPPIST-South

We used the 60cm robotic telescope TRAPPIST-South (TRansiting Planets and Planetesimals Small Telescope; Gillon et al. 2011; Jehin et al. 2011) at La Silla (Chile) to observe a partial transit of WASP-161 b in the Sloan- z' filter on 28 Jan 2016, two partial transits of WASP-163 b in a broad $I + z$ filter (transmittance $>90\%$ from 750 nm to beyond $1 \mu\text{m}$) on 6 Sep 2014 and 5 July 2016, and two transits (one full + one partial) of WASP-170 b in $I + z$ on 25 Dec 2015 and 26 Feb 2017. TRAPPIST-South is equipped with a thermoelectrically-cooled $2K \times 2K$ CCD having a pixel scale of $0.65''$ that translates into a $22' \times 22'$ field of view. Standard calibration of the images, fluxes extraction and differential photometry were then performed as described in Gillon et al. (2013). The resulting light curves are shown in Fig. 2, 3, and 4.

2.2.3. EulerCam

We used the EulerCam camera (Lendl et al. 2012) on the 1.2m Euler-Swiss telescope (La Silla, Chile) to observe a transit of WASP-163 b on 27 July 2016 in the RG filter, and also a transit of WASP-170 b on 20 Dec 2016 in the broad NGTS filter ($\lambda_{NGTS} = [500 - 900\text{nm}]$, Wheatley et al. 2017). The detector of EulerCam is an $e2v$ $4k \times 4k$ back-illuminated deep-depletion silicon CCD. Its field of view is $15.7' \times 15.7'$, and its pixel scale is $0.23''$. The calibration and photometric reduction (aperture + differential photometry) of the images were performed as described by Lendl et al. (2012). The resulting light curves are shown in Fig. 3 and 4.

2.2.4. NITES

Two transits of WASP-163 b were observed with the 0.4m NITES (Near-Infrared Transiting ExoplanetS Telescope, McCormac et al. 2014) robotic telescope at La Palma (Canary Islands). The first transit was full and observed in R-band on 27 June 2016, while the second was only partial and observed in I-band on 10 July 2016. NITES is equipped with a thermoelectrically-cooled 1024×1024 CCD camera that has a pixel scale of $0.66''$ that translates into a field of view of $11.3' \times 11.3'$. The data were reduced in PYTHON using CCDPROC (Craig et al. 2015). A master bias, dark and flat was created using the standard process on each night. A minimum of 21 of each frame was used in each master calibration frame. Non-variable nearby comparison stars were selected by hand and aperture photometry extracted using SEP (Barbary 2016; Bertin and Arnouts 1996). The shift between each defocused image was measured using the DONUTS algorithm (McCormac et al. 2013) and the photometry apertures were recentered. The resulting light curves are shown in Fig. 3.

2.2.5. SPECULOOS-South

One transit of WASP-161 b was observed with Europa, one of the four telescopes of the SPECULOOS-South facility (Burdanov et al. 2017; Gillon 2018; Delrez et al. 2018), which is currently being commissioned at ESO Paranal Observatory (Chile). Each telescope is a robotic Ritchey-Chretien (F/8) telescope of 1-m diameter. They are equipped

with Andor Peltier-cooled deeply depleted 2K×2K CCD cameras, with good sensitivities in the very-near-infrared up to 1 μm . The field of view of each telescope is 12'×12' and the pixel scale is 0.35"/pixel. The transit was observed on 5 Jan 2018 in the Sloan- z' filter. The calibration and photometric reduction of the data were performed as described in Gillon et al. (2013). The resulting light curve is shown in Fig. 2.

2.3. Spectroscopy and radial velocities

Radial velocity (RV) measurements were performed for the three stars with the CORALIE spectrograph (Queloz et al. 2000) mounted on the 1.2-meter Euler-Swiss telescope at ESO La Silla Observatory in Chile. We obtained 24 spectroscopic measurements for WASP-161 between December 2014 and January 2017; 25 spectroscopic measurements for WASP-163 between June 2015 and May 2017; and 20 spectroscopic measurements for WASP-170 between February 2015 and May 2017. For all spectroscopic observations, RV were obtained using the cross-correlation technique described in Baranne et al. (1996). The RV time-series for WASP-161, WASP-163 and WASP-170 shows clear sinusoidal signals with periods and phases in good agreement with those deduced from the WASP transit detections. Those radial velocity measurements are presented in the table 6.

The bisector spans (Queloz et al. 2001) of the CORALIE cross-correlation function (CCF) revealed to be stable, their standard deviations being close to their average errors (122 *vs* 80 ms^{-1} for WASP-161, 116 *vs* 125 ms^{-1} for WASP-163, and 87 *vs* 97 ms^{-1} for WASP-170). No evidence for a correlation between the RVs and the bisector spans was found (Fig. 2, 3, and 4), which is consistent with the planetary nature of the transiting bodies.

3. ANALYSIS

3.1. Spectroscopic analysis

We co-added the CORALIE spectra to produce single spectra with average signal-to-noise between 50 and 100. From these spectra, we determined the stellar effective temperature T_{eff} , surface gravity $\log g$, lithium abundance $\log A(\text{Li})$, metallicity $[Fe/H]$, and rotational velocity $v \sin i$ of the stars, following the method described by Doyle et al. (2013). To constrain $v \sin i$, we assumed macroturbulence values of 5.31 km.s^{-1} , 3.59 km.s^{-1} and 3.74 km.s^{-1} for WASP-161, WASP-163 and WASP-170 respectively using the Doyle et al. (2014) calibration.

3.2. Global modeling of the data

To determinate the stellar and planetary parameters of each system, we performed a global analysis of the follow-up photometry (Table 3) and CORALIE RVs (Table 6) using the adaptative Markov chain Monte-Carlo (MCMC) code described by Gillon et al. (2012). The CORALIE RVs were modeled with a classical Keplerian model (e.g. Murray and Correia 2010). Each light curve was represented by the transit model of Mandel and Agol (2002), assuming a quadratic limb-darkening law, multiplied by a baseline model consisting of a polynomial function of one or several external parameters (time, background, airmass, etc., see Table 3). The selection of these baseline model was based on the minimization of the BIC (Bayesian Information Criterium, Schwarz 1978).

TRAPPIST-North and TRAPPIST-South telescopes are equipped with German equatorial mounts that have to perform 180° flips when the target crosses the meridian during the observations. These rotations result in different positions on the detector of the stellar images before and after the meridian crossing. For the corresponding light curves, a normalization offset at the time of the flip was introduced in the baseline model (Table 3).

For each system, the "jump" parameters of the MCMC, i.e. the parameters perturbed at each step of the Markov chains, were: the transit depth $dF = (R_p/R_*)^2$, the transit impact parameter $b = a \cos i/R_*$ (with a the orbital semi-major axis and i the inclination of the orbit), the transit duration W , the mid-transit time T_0 , the orbital period P , the parameters $\sqrt{e} \cos \omega$ and $\sqrt{e} \sin \omega$ (with ω the argument of periastron and e the orbital eccentricity), the modified RV semi-amplitude $K2 = K\sqrt{1 - e^2}P^{1/3}$ (with K is the RV semi-amplitude), the stellar effective temperature T_{eff} , and the stellar metallicity $[Fe/H]$. In addition, for each filter, the combinations, $c_1 = 2 \times u_1 + u_2$ and $c_2 = u_1 - 2 \times u_2$ were also jump parameters, u_1 and u_2 being the linear and quadratic limb-darkening coefficients. Normal prior probability distribution functions (PDFs) based on the theoretical tables of Claret (2000) were assumed for u_1 and u_2 (Table 5). Each analysis was composed of three Markov chains of 10^5 steps, the first 20% of each chain being considered as its burn-in phase and discarded. The convergence of the Markov chains was checked using the statistical test presented by Gelman and Rubin (1992). The correlated noise present in the light curves was taken into account as described by Gillon et al. (2012), by comparing the scatters of the residuals in the original and in time-binned versions of the data, and by rescaling the errors accordingly. For the RVs, jitter noises of 32.6 m.s^{-1} (WASP-161), 54.1 m.s^{-1} (WASP-163),

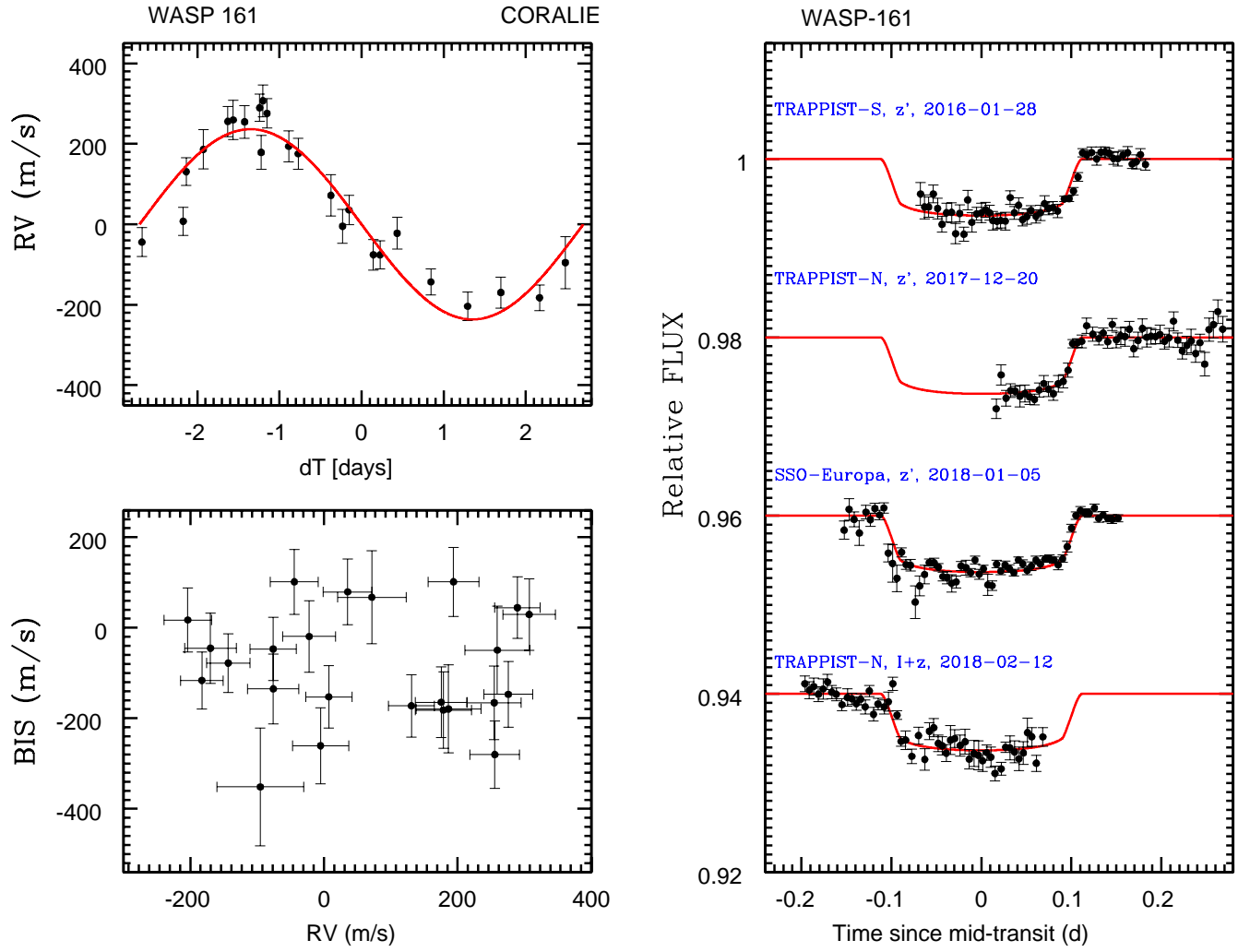


Figure 2. *Right-hand panel:* Individual follow-up transit light curves for WASP-161 b. The observations are shown as black points (bin width = 7.2 min) and are period-folded on the best-fit transit ephemeris. The solid red lines are our best-fit transit models. The light curves are shifted along the y -axis for clarity. Both the data and the models are divided by the best-fit baseline model (i.e. detrended). *Left-hand panel top:* CORALIE RVs for WASP-161 phase-folded on the best-fit orbital period with the best-fit Keplerian model in red. *Left-hand panel bottom:* bisector spans (BIS) *vs* RVs diagram.

and 42.8 m.s^{-1} (WASP-170) were added quadratically to the error bars, to equalize the mean errors with the rms of the best-fitting model residuals.

At each step of the Markov chains, the values drawn for T_{eff} , and $[Fe/H]$, and the dynamical stellar density ρ_* (as deduced from the jump parameters dF , b , W , P , $\sqrt{e} \cos \omega$, and $\sqrt{e} \sin \omega$; see, e.g., Winn 2010) are used to determine a value for the stellar mass M_* with an empirical law (Enoch et al. 2010) calibrated using the parameters of an extensive list of well characterized eclipsing binary systems. The stellar radius and the planets physical parameters can then be computed. Two MCMC analyses were performed for each system, one assuming an eccentric orbit and one assuming a circular one. Using the BIC as proxy for the model marginal likelihood, the resulting Bayes factors were largely (> 1000) in favor of a circular model for all systems. We thus adopted the circular solution for the three planets. These solutions are presented in Table 1.

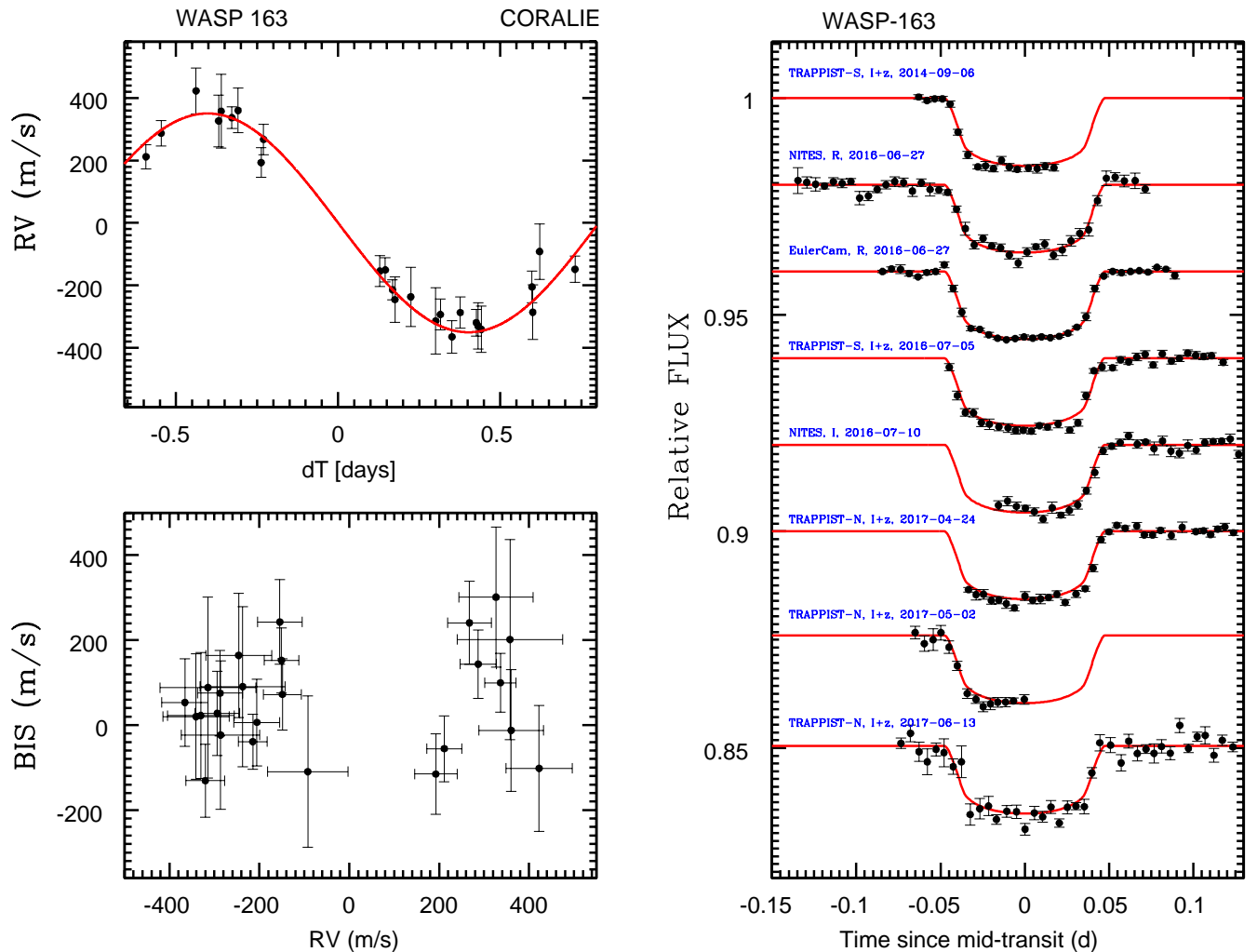


Figure 3. Same as Fig. 2 but for WASP-163.

4. ROTATION PERIODS

The WASP light curves of WASP-170 show a quasi-periodic modulation with an amplitude of about 0.6 per cent and a period of about 7.8 days. We assume this is due to the combination of the stars rotation and magnetic activity, i.e., star spots. We used the sine-wave fitting method described in Maxted et al. (2011) to refine this estimate of the amplitude and period of the modulation. Variability due to star spots is not expected to be coherent on long timescales as a consequence of the finite lifetime of star-spots and differential rotation in the photosphere so we analysed each season of data for WASP-170 separately. We also analyse the data from each camera used to observe WASP-170 separately so that we can assess the reliability of the results. We removed the transit signal from the data prior to calculating the periodograms by subtracting a simple transit model from the lightcurve. We calculated periodograms over 8192 uniformly spaced frequencies from 0 to 1.5 cycles/day. The false alarm probability (FAP) is calculated using a boot-strap Monte Carlo method also described in Maxted et al. (2011). The results are given in Table 2 and the periodograms and lightcurves are shown in Fig. 5. There is a clear signal near 7.8 days in 5 out of 7 data sets, from which we obtain a value for the rotation period of $P_{rot} = 7.75 \pm 0.02$ d. This rotation period together with our estimate for the stellar radius implies a value of $V_{rot} \sin I = 6.1 \pm 0.3$ km s⁻¹, assuming that the rotation axis of the

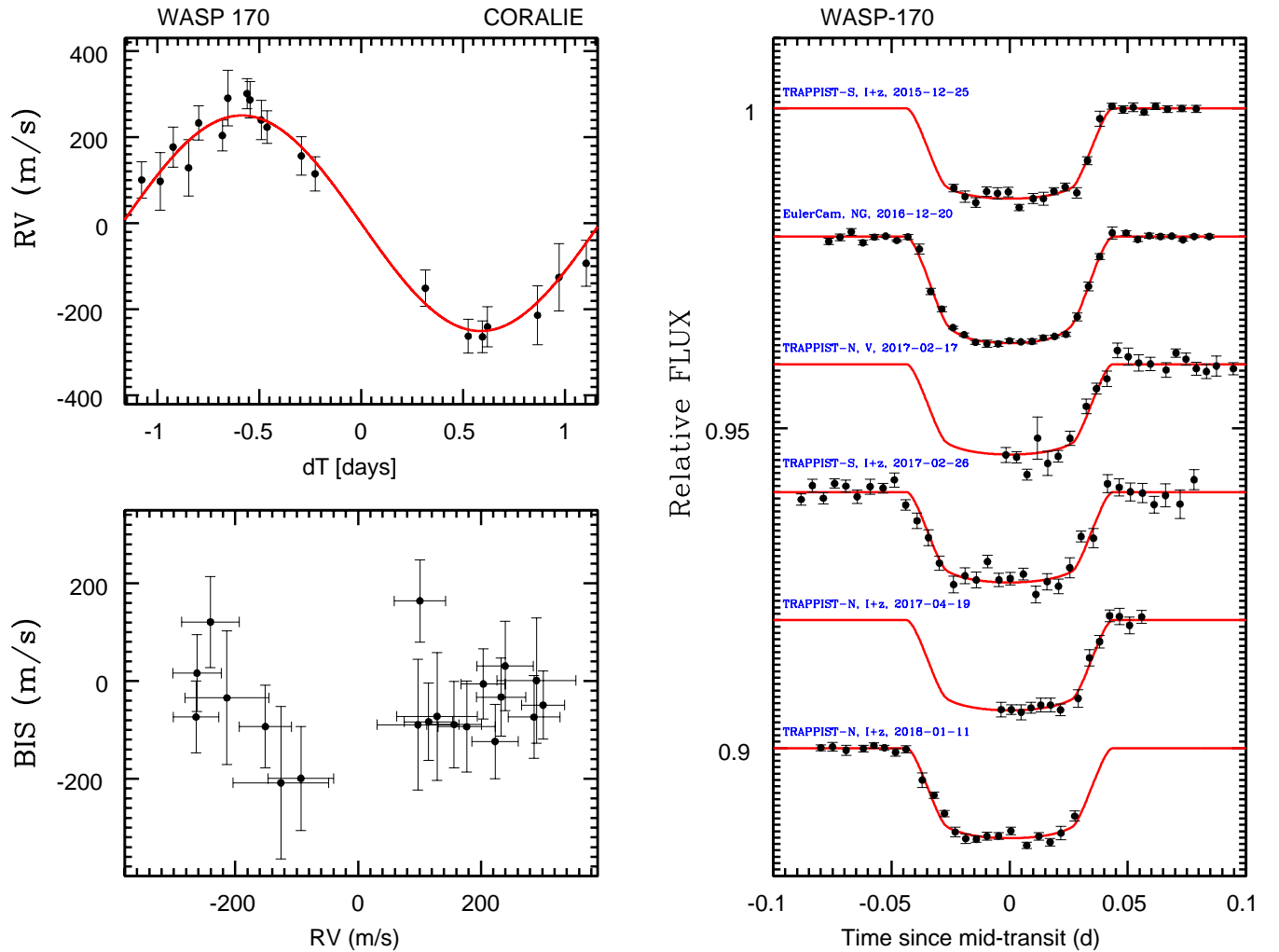


Figure 4. same as Fig. 2 but for WASP-170.

star is approximately aligned with the orbital axis of the planet, in the good agreement with the spectroscopic analysis ($v \sin i = 5.6 \pm 1.0 \text{ km s}^{-1}$, see table 1). We used a least-squares fit of a sinusoidal function and its first harmonic to model the rotational modulation in the lightcurves for each camera and season with the rotation period fixed at $P_{rot} = 7.75 \text{ d}$.

For WASP-161 and WASP-163 a similar analysis leads to upper limits of 0.6 millimagnitudes and 2.0 millimagnitudes with 95 per cent confidence for the amplitude of any sinusoidal signal over the same frequency range, respectively.

5. STELLAR EVOLUTION MODELING

We also used the open source software BAGEMASS¹ to calculate the posterior mass distribution for each star using the Bayesian method described by Maxted et al. (2015). The models used in BAGEMASS were calculated using the GARSTEC stellar evolution code (Weiss and Schlattl 2008). The mass and age of the stars derived are shown in Table 4, in good agreement with the mass-calibration from MCMC analysis (see Table 1).

¹ <http://sourceforge.net/projects/bagemass>

Camera	Dates	N	P [d]	a [mmag]	FAP
227	4846-4943	4899	7.780	0.010	$< 10^{-4}$
227	5567-5675	2407	3.978	0.005	0.15
227	5913-6041	2794	7.725	0.007	$< 10^{-4}$
228	4846-4943	5283	7.703	0.011	$< 10^{-4}$
228	5212-5308	4747	7.813	0.006	0.002
228	5613-5676	2651	4.073	0.003	1.00
228	5913-6041	3649	7.747	0.008	$< 10^{-4}$

Table 2. Periodogram analysis of the WASP lightcurves for WASP-170. Observing dates are JD-2450000, N is the number of observations used in the analysis, a is the semi-amplitude of the best-fit sine wave at the period P found in the periodogram with false-alarm probability FAP.

Target	Night	Telescope	Filter	N_p	T_{exp} (s)	Baseline function	σ (%)	$\sigma_{7.2m}$ (%)	β_w	β_r	CF
WASP-161	2016-01-28	TRAPPIST-S	Sloan- z'	938	10	$p(t + xy + o)$	0.37	0.051	1.29	1.08	1.39
WASP-161	2017-12-20	TRAPPIST-N	Sloan- z'	902	10	$p(t + b)$	0.43	0.072	1.14	1.05	1.20
WASP-161	2018-01-05	SPECULOOS	Sloan- z'	1235	10	$p(xy)$	0.44	0.087	1.22	1.44	1.72
WASP-161	2018-02-12	TRAPPIST-N	Sloan- z'	892	10	$p(a)$	0.46	0.054	1.14	1.20	1.37
WASP-163	2014-09-06	TRAPPIST-S	$I + z$	345	12	$p(t)$	0.33	0.006	1.06	1.00	1.06
WASP-163	2016-06-27	NITES	Johnson-R	443	30	$p(t)$	0.41	0.012	1.71	1.00	1.71
WASP-163	2016-06-27	EulerCam	RG	170	60	$p(t + f + b)$	0.11	0.005	1.20	1.10	1.31
WASP-163	2016-07-05	TRAPPIST-S	$I + z$	602	12	$p(a + xy)$	0.35	0.011	1.16	1.35	1.56
WASP-163	2016-07-10	NITES	Johnson-I	388	30	$p(t)$	0.58	0.012	1.55	1.18	1.83
WASP-163	2017-04-24	TRAPPIST-N	$I + z$	487	12	$p(t + xy + o)$	0.31	0.008	1.02	1.07	1.09
WASP-163	2017-05-02	TRAPPIST-N	$I + z$	213	12	$p(b)$	0.54	0.009	0.90	1.00	0.90
WASP-163	2017-06-13	TRAPPIST-N	$I + z$	557	14	$p(t + f)$	0.69	0.021	0.87	1.16	1.01
WASP-170	2015-12-25	TRAPPIST-S	$I + z$	359	15	$p(f)$	0.29	0.008	1.04	1.05	1.09
WASP-170	2016-12-20	EulerCam	NGTS	207	40	$p(t)$	0.11	0.005	1.49	1.13	1.68
WASP-170	2017-02-17	TRAPPIST-N	Johnson-V	239	20	$p(t)$	0.46	0.013	1.22	1.00	1.22
WASP-170	2017-02-26	TRAPPIST-S	$I + z$	545	15	$p(t + a)$	0.51	0.015	1.32	1.16	1.53
WASP-170	2017-04-19	TRAPPIST-N	$I + z$	186	15	$p(a + xy)$	0.41	0.008	0.99	1.00	0.99
WASP-170	2018-01-11	TRAPPIST-N	$I + z$	315	15	$p(t)$	0.26	0.007	0.75	1.11	0.83

Table 3. For each light curve used in this work, the table shows the date of acquisition, the used telescope and filter, the number of data points, the exposure time, the selected baseline function, the standard deviation of the best-fit residuals, the deduced values for β_w , β_r and $CF = \beta_w \times \beta_r$. For the baseline function, $p(\epsilon^N)$, denotes, respectively, a N -order polynomial function of time ($\epsilon = t$), airmass ($\epsilon = a$), full-width at half maximum ($\epsilon = f$), background ($\epsilon = b$), and x and y positions ($\epsilon = xy$). The symbol o demotes an offset fixed at the time of the meridian flip.

6. DISCUSSION

Table 4. Stellar mass and age estimates. The mean and standard deviation of the posterior distributions are given together with the best-fit values in parentheses.

Star	Mass [M_{\odot}]	Age [Gyr]
WASP-161 A	1.42 ± 0.05 (1.40)	2.4 ± 0.4 (2.4)
WASP-163 A	0.87 ± 0.06 (0.78)	11.4 ± 3.5 (17.4) [†]
WASP-170 A	0.99 ± 0.07 (1.03)	4.8 ± 3.1 (2.9)

[†] Best fit occurs at edge of model grid.

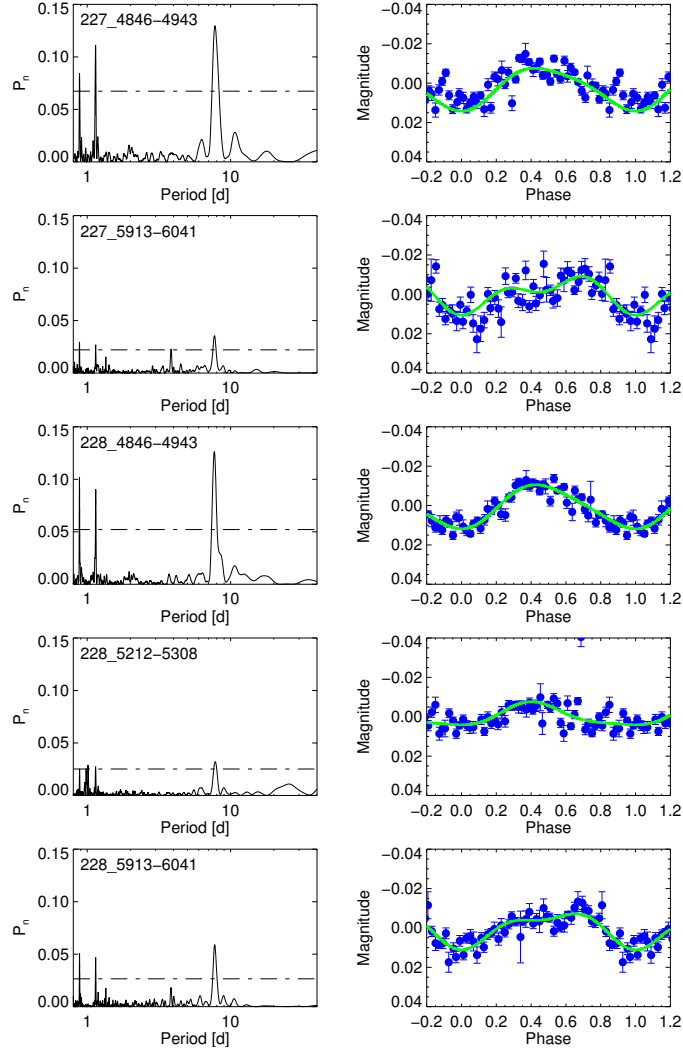


Figure 5. Left: Periodograms of WASP-170. Horizontal lines indicate false-alarm probability levels 0.1, 0.01 and 0.001. Right: Lightcurves phase-binned on the assumed rotation period of 7.75 days (points) with second-order harmonic series fit by least squares (lines). Plots are labelled by camera number and date range as noted in Table 2.

WASP-161 b, WASP-163 b and WASP-170 b are planets slightly larger ($1.14 \pm 0.06 R_{Jup}$, $1.2 \pm 0.1 R_{Jup}$, and $1.10 \pm 0.09 R_{Jup}$) and more massive ($2.5 \pm 0.2 M_{Jup}$, $1.9 \pm 0.2 M_{Jup}$, and $1.6 \pm 0.2 M_{Jup}$) than Jupiter. Given their masses and their large irradiances (Fig. 6 a), their radii are well reproduced by the models of Fortney et al. (2007), assuming a core mass of a few dozens of M_{\oplus} and ages larger than a few hundreds Myr (Fig. 6 b).

The empirical relationship derived by Weiss et al. (2013) for planets more massive than $150M_{\oplus}$, $R_p/R_{\oplus} = 2.45(M_p/M_{\oplus})^{-0.039 \pm 0.01}(F/\text{erg s}^{-1}\text{cm}^{-2})^{0.094}$ predicts radii of $1.16 \pm 0.30 R_{Jup}$, $1.20 \pm 0.34 R_{Jup}$ and $1.15 \pm 0.31 R_{Jup}$ for WASP-161 b, 163 b, and 170 b, respectively, which are consistent with our measured radii. The three new

LD coefficient	WASP-161	WASP-163	WASP-170
$u_{1,z'}$	0.184 ± 0.011	-	-
$u_{2,z'}$	0.300 ± 0.005	-	-
$u_{1,I+z}$	-	0.207 ± 0.012	0.2539 ± 0.0202
$u_{2,I+z}$	-	0.297 ± 0.010	0.2788 ± 0.0152
$u_{1,Johnson-I}$	-	0.331 ± 0.034	0.2727 ± 0.0321
$u_{2,Johnson-I}$	-	0.251 ± 0.019	0.2805 ± 0.0158
$u_{1,Johnson-R}$	-	0.420 ± 0.043	-
$u_{2,Johnson-R}$	-	0.248 ± 0.027	-
$u_{1,Johnson-V}$	-	-	0.437 ± 0.044
$u_{2,Johnson-V}$	-	-	0.271 ± 0.025

Table 5. Expectations and standard deviations of the normal distributions used as prior PDFs for the quadratic limb-darkening (LD) coefficients u_1 and u_2 in our MCMC analyses.

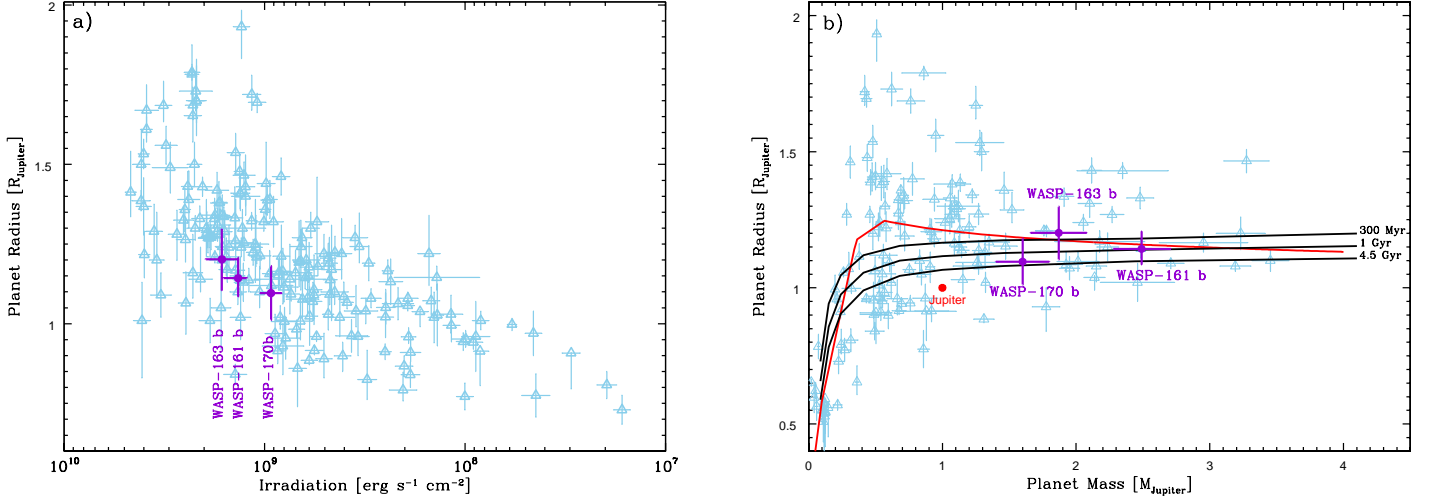


Figure 6. **a)**: Irradiation-radius diagram and **b)**: mass-radius diagram for the known transiting planets with masses ranging from 0. to $4. M_{Jupiter}$ (data from exoplanets.org) are shown as skyblue triangles with error bars). The planets WASP-161 b, WASP-163 b and WASP-170 b are shown in violet. In **b)** the black lines present models of irradiated giant planets with semi-major axes of 0.045 AU, core masses of $25 M_{\oplus}$, and ages of 300 Myrs, 1 Gyrs and 4.5 Gyrs (Fortney et al. 2007). The empirical law of Weiss et al. (2013) is also plotted as a red line.

planets whose discovery is described appear thus to be 'standard' hot Jupiters that do not present a 'radius anomaly' challenging standard models of irradiated gas giants.

The discovery of WASP-161 b, WASP-163 b, and WASP-170 b establishes the new robotic telescope TRAPPIST-North as a powerful Northern facility for the photometric follow-up of transiting exoplanet candidates found by ground-based wide-field surveys like WASP, and soon by the space-based mission TESS (Ricker et al. 2016).

7. ACKNOWLEDGEMENT

WASP-South is hosted by the South African Astronomical Observatory and we are grateful for their ongoing support and assistance. Funding for WASP comes from consortium universities and from the UK's Science and Technology Facilities Council. The Euler Swiss telescope is supported by the Swiss National Science Foundation. TRAPPIST-South is funded by the Belgian Fund for Scientific Research (Fond National de la Recherche Scientifique, FNRS) under the grant FRFC 2.5.594.09.F, with the participation of the Swiss National Science Foundation (SNF). MG is FNRS Research Associate, and EJ is FNRS Senior Research Associate. LD acknowledges support from the Gruber Foundation Fellowship. The research leading to these results has received funding from the European Research Council under the

FP/2007-2013 ERC Grant Agreement 336480, and from the ARC grant for Concerted Research Actions, financed by the Wallonia-Brussels Federation. This work was also partially supported by a grant from the Simons Foundation (ID 327127 to Didier Queloz), a grant from the Erasmus+ International Credit Mobility programme (K Barkaoui), as well as by the MERAC foundation (PI Triaud).

Target	HID - 2,450,000	RV (km s ⁻¹)	σ_{RV} (km s ⁻¹)	BS (km s ⁻¹)	Target	HID - 2,450,000	RV (km s ⁻¹)	σ_{RV} (km s ⁻¹)	BS (km s ⁻¹)
WASP-163	7193.741864	-37.28368	0.11764	-0.05553	WASP-161	6995.779435	37.47673	0.03954	0.10140
WASP-163	7194.544082	-37.93075	0.07383	0.14349	WASP-161	7404.735111	37.93140	0.04051	-0.15260
WASP-163	7221.642393	-37.90136	0.07320	-0.10196	WASP-161	7421.604076	37.83967	0.03886	-0.17254
WASP-163	7264.560197	-37.21532	0.08258	0.30132	WASP-161	7422.600890	37.60262	0.03490	-0.17929
WASP-163	7265.528948	-37.85780	0.08717	0.20131	WASP-161	7423.668930	37.52064	0.03555	-0.28021
WASP-163	7268.579849	-37.96344	0.07401	0.09958	WASP-161	7425.646222	37.72356	0.03456	-0.04948
WASP-163	7276.497340	-37.95927	0.10641	-0.01258	WASP-161	7426.579130	37.96837	0.03946	-0.16563
WASP-163	7277.497313	-37.30844	0.07177	-0.11522	WASP-161	7428.627488	37.41733	0.03252	0.04443
WASP-163	7292.517764	-37.82511	0.09442	0.24068	WASP-161	7451.572650	37.47357	0.03171	-0.18188
WASP-163	7293.464761	-37.14368	0.07405	0.24267	WASP-161	7452.635935	37.57245	0.03459	0.02944
WASP-163	7294.524814	-37.73113	0.08910	0.15248	WASP-161	7453.567361	37.93838	0.03395	-0.14701
WASP-163	7484.863204	-37.46746	0.03879	-0.03903	WASP-161	7457.538982	37.46129	0.03590	0.10144
WASP-163	7486.827998	-37.42444	0.04741	0.16399	WASP-161	7481.604825	37.65253	0.04218	-0.16457
WASP-163	7487.796538	-37.79839	0.04198	0.09038	WASP-161	7485.611602	37.80633	0.03723	0.06739
WASP-163	7488.843232	-37.86941	0.03227	0.08838	WASP-161	7669.874869	37.96450	0.03643	-0.26075
WASP-163	7523.858463	-37.41079	0.04884	0.02768	WASP-161	7670.873488	37.54791	0.03644	0.07926
WASP-163	7567.695488	-37.80440	0.03823	0.05318	WASP-161	7674.868344	37.89486	0.04877	-0.13512
WASP-163	7569.757824	-37.85478	0.05104	0.07520	WASP-161	7716.752403	37.48642	0.06487	-0.04681
WASP-163	7575.726750	-37.81565	0.04977	-0.13093	WASP-161	7717.747923	37.75662	0.04854	-0.01920
WASP-163	7576.662344	-37.38270	0.04033	0.02235	WASP-161	7718.788841	37.80035	0.03818	-0.07805
WASP-163	7577.523403	-37.95890	0.04961	0.01980	WASP-161	7726.778064	37.39224	0.03876	0.01718
WASP-163	7593.681424	-37.95775	0.05024	0.00629	WASP-161	7746.846331	37.51936	0.03845	-0.04507
WASP-163	7652.535369	-37.33184	0.03470	-0.02346	WASP-161	7751.735303	37.69111	0.05137	-0.11653
WASP-163	7823.841592	-38.04752	0.05155	-0.10981	WASP-161	7761.696319	37.93171	0.04203	-0.35162
WASP-163	7894.742995	-37.97268	0.04302	0.07214					
WASP-170	7066.749515	30.67098	0.04671	0.16402	WASP-170	7753.676136	30.70862	0.03924	-0.12366
WASP-170	7686.843189	31.25138	0.06427	-0.08954	WASP-170	7754.698984	31.19850	0.04009	-0.08925
WASP-170	7694.846421	30.81621	0.04224	-0.09353	WASP-170	7759.695126	31.20223	0.04579	-0.08356
WASP-170	7719.778573	31.25569	0.04232	-0.07239	WASP-170	7760.780900	30.70044	0.03683	-0.09317
WASP-170	7721.746763	31.13284	0.04660	-0.03291	WASP-170	7773.792434	31.17400	0.03803	0.01621
WASP-170	7723.773046	30.84403	0.05319	-0.00621	WASP-170	7801.545185	31.08175	0.06548	-0.07362
WASP-170	7724.787756	31.05367	0.03945	0.00095	WASP-170	7812.635803	30.67711	0.06835	0.12073
WASP-170	7726.799025	31.25678	0.03495	-0.04931	WASP-170	7825.546120	31.14228	0.04425	-0.03448
WASP-170	7747.780705	31.16081	0.03596	-0.07385	WASP-170	7859.637199	30.88820	0.07800	-0.20830
WASP-170	7749.729288	31.01646	0.04208	0.03075	WASP-170	7883.473343	31.07842	0.06692	-0.19927

Table 6. CORALIE radial-velocity measurements for WASP-161, WASP-163 and WASP-170 (BS = bisector spans).

REFERENCES

Mayor, M.; Queloz, D. *Nature* **1995**, *378*, 355–359.

Charbonneau, D.; Brown, T. M.; Latham, D. W.;

Mayor, M. *ApJL* **2000**, *529*, L45–L48.

- Henry, G. W.; Marcy, G. W.; Butler, R. P.; Vogt, S. S. *ApJL* **2000**, *529*, L41–L44.
- Winn, J. N.; Fabrycky, D. C. *ARA&A* **2015**, *53*, 409–447.
- Fortney, J. J.; Marley, M. S.; Barnes, J. W. *ApJ* **2007**, *659*, 1661–1672.
- Correia, A. C. M.; Laskar, J. *Icarus* **2010**, *205*, 338–355.
- Chang, C.; Liu, G. Z.; Tang, C. X.; Chen, C. H.; Shao, H.; Huang, W. H. *Applied Physics Letters* **2010**, *96*, 111502.
- Winn, J. N. *ArXiv e-prints* **2010**,
- Deming, D.; Seager, S. *Nature* **2009**, *462*, 301–306.
- Seager, S.; Deming, D. *ARA&A* **2010**, *48*, 631–672.
- Sing, D. K. et al. *Nature* **2016**, *529*, 59–62.
- Crossfield, I. J. M. *PASP* **2015**, *127*, 941.
- Pollacco, D. L. et al. *Publications of the Astronomical Society of the Pacific* **2006**, *118*, 1407–1418.
- Collier Cameron, A. et al. *MNRAS* **2007**, *380*, 1230–1244.
- Hellier, C.; Anderson, D. R.; Collier-Cameron, A.; Miller, G. R. M.; Queloz, D.; Smalley, B.; Southworth, J.; Triaud, A. H. M. J. *ApJL* **2011**, *730*, L31.
- Hellier, C. et al. *MNRAS* **2012**, *426*, 739–750.
- Collier Cameron, A. et al. *MNRAS* **2006**, *373*, 799–810.
- Collier Cameron, A. et al. *MNRAS* **2007**, *380*, 1230–1244.
- Gillon, M. et al. *Nature* **2017**, *542*, 456–460.
- Gillon, M. *Nature Astronomy* **2018**, *2*, 344–344.
- Burdanov, A.; Delrez, L.; Gillon, M.; Jehin, E.; Speculoos, T.; Trappist Teams, *Handbook of Exoplanets, Edited by Hans J. Deeg and Juan Antonio Belmonte. Springer Living Reference Work, ISBN: 978-3-319-30648-3, 2017, id.130*; 2017; p 130.
- Delrez, L. et al. *ArXiv e-prints* **2018**,
- Bonfils, X.; Gillon, M.; Forveille, T.; Delfosse, X.; Deming, D.; Demory, B.-O.; Lovis, C.; Mayor, M.; Neves, V.; Perrier, C.; Santos, N. C.; Seager, S.; Udry, S.; Boisse, I.; Bonnefoy, M. *A&A* **2011**, *528*, A111.
- Gillon, M. et al. *A&A* **2012**, *542*, A4.
- Delrez, L. et al. *A&A* **2014**, *563*, A143.
- Jehin, E.; Gillon, M.; Queloz, D.; Magain, P.; Manfroid, J.; Chantry, V.; Lendl, M.; Hutsemékers, D.; Udry, S. *The Messenger* **2011**, *145*, 2–6.
- Gillon, M. et al. *A&A* **2013**, *552*, A82.
- Gillon, M.; Jehin, E.; Magain, P.; Chantry, V.; Hutsemékers, D.; Manfroid, J.; Queloz, D.; Udry, S. *EPJ Web of Conferences* **2011**, *11*, 06002.
- Lendl, M. et al. *Astronomy & Astrophysics* **2012**, *544*, A72.
- Wheatley, P. J. et al. *ArXiv e-prints* **2017**,
- McCormac, J.; Skillen, I.; Pollacco, D.; Faedi, F.; Ramsay, G.; Dhillon, V. S.; Todd, I.; Gonzalez, A. *Monthly Notices of the Royal Astronomical Society* **2014**, *438*, 3383–3398.
- Craig, M. W. et al. ccdproc: CCD data reduction software. Astrophysics Source Code Library, 2015.
- Barbary, K. *The Journal of Open Source Software* **2016**, *1*, 1.
- Bertin, E.; Arnouts, S. *A&AS* **1996**, *117*, 393–404.
- McCormac, J.; Pollacco, D.; Skillen, I.; Faedi, F.; Todd, I.; Watson, C. A. *PASP* **2013**, *125*, 548.
- Queloz, D.; Mayor, M.; Naef, D.; Santos, N.; Udry, S.; Burnet, M.; Confino, B. **2000**, 548.
- Baranne, A.; Queloz, D.; Mayor, M.; Adrianzyk, G.; Knispel, G.; Kohler, D.; Lacroix, D.; Meunier, J.-P.; Rimbaud, G.; Vin, A. *A&AS* **1996**, *119*, 373–390.
- Queloz, D.; Henry, G. W.; Sivan, J. P.; Baliunas, S. L.; Beuzit, J. L.; Donahue, R. A.; Mayor, M.; Naef, D.; Perrier, C.; Udry, S. *A&A* **2001**, *379*, 279–287.
- Doyle, A. P.; Smalley, B.; Maxted, P. F. L.; Anderson, D. R.; Cameron, A. C.; Gillon, M.; Hellier, C.; Pollacco, D.; Queloz, D.; Triaud, A. H. M. J.; West, R. G. *MNRAS* **2013**, *428*, 3164–3172.
- Doyle, A. P.; Davies, G. R.; Smalley, B.; Chaplin, W. J.; Elsworth, Y. *MNRAS* **2014**, *444*, 3592–3602.
- Murray, C. D.; Correia, A. C. M. In *Exoplanets*; Seager, S., Ed.; 2010; pp 15–23.
- Mandel, K.; Agol, E. *ApJL* **2002**, *580*, L171–L175.
- Schwarz, G. *Ann. Statist.* **1978**, *6*, 461–464.
- Claret, A. *VizieR Online Data Catalog* **2000**, *336*.
- Gelman, A.; Rubin, D. B. *Statistical Science* **1992**, *7*, 457–472.
- Enoch, B.; Collier Cameron, A.; Parley, N. R.; Hebb, L. *A&A* **2010**, *516*, A33.
- Maxted, P. F. L. et al. *PASP* **2011**, *123*, 547.
- Maxted, P. F. L.; Serenelli, A. M.; Southworth, J. *A&A* **2015**, *575*, A36.
- Weiss, A.; Schlattl, H. *Ap&SS* **2008**, *316*, 99–106.
- Weiss, L. M. et al. *ApJ* **2013**, *768*, 14.
- Ricker, G. R. et al. The Transiting Exoplanet Survey Satellite. Space Telescopes and Instrumentation 2016: Optical, Infrared, and Millimeter Wave. 2016; p 99042B.